1999

Computational Fluid Dynamics Simulation of Chemical Reactors: Application of in Situ Adaptive Tabulation to Methane Thermochlorination Chemistry

Jimmy J. Shah
Iowa State University

Rodney O. Fox
Iowa State University, rofox@iastate.edu

Computational Fluid Dynamics Simulation of Chemical Reactors: Application of in Situ Adaptive Tabulation to Methane Thermochlorination Chemistry

Abstract

Recently, a novel algorithmin situ adaptive tabulationhas been proposed to effectively incorporate detailed chemistry in computational fluid dynamics (CFD) simulations for turbulent reacting flows. In this work, detailed tests performed on a pairwise-mixing stirred reactor (PMSR) model are presented implementing methane thermochlorination chemistry to validate the in situ adaptive tabulation (ISAT) algorithm. The detailed kinetic scheme involves 3 elements (H, C, Cl) and 38 chemical species undergoing a total of 152 elementary reactions. The various performance issues (error control, accuracy, storage requirements, speed-up) involved in the implementation of detailed chemistry in particle-based methods (full PDF methods) are discussed. Using an error tolerance of εtol = 2 ? 10-4, sufficiently accurate results with minimal storage requirements and significantly less computational time than would be required with direct integration are obtained. Based on numerous test simulations, an error tolerance in the range of 10-3?10-4 is found to be satisfactory for carrying out full PDF simulations of methane thermochlorination reactors. The results presented here demonstrate that the implementation of ISAT makes possible the hitherto formidable task of implementing detailed chemistry in CFD simulations of methane thermochlorination reactors.

Disciplines

Catalysis and Reaction Engineering | Chemical Engineering

Comments

This article is from *Industrial & Engineering Chemistry Research*38(1999):4200-4212, doi:10.1021/ie990125g. Posted with permission.

Computational Fluid Dynamics Simulation of Chemical Reactors: Application of in Situ Adaptive Tabulation to Methane Thermochlorination Chemistry

Jimmy J. Shah and Rodney O. Fox*

Department of Chemical Engineering, Iowa State University, Ames, Iowa 50011-2230

Recently, a novel algorithm—in situ adaptive tabulation—has been proposed to effectively incorporate detailed chemistry in computational fluid dynamics (CFD) simulations for turbulent reacting flows. In this work, detailed tests performed on a pairwise-mixing stirred reactor (PMSR) model are presented implementing methane thermochlorination chemistry to validate the in situ adaptive tabulation (ISAT) algorithm. The detailed kinetic scheme involves 3 elements (H, C, Cl) and 38 chemical species undergoing a total of 152 elementary reactions. The various performance issues (error control, accuracy, storage requirements, speed-up) involved in the implementation of detailed chemistry in particle-based methods (full PDF methods) are discussed. Using an error tolerance of $\epsilon_{tol} = 2 \times 10^{-4}$, sufficiently accurate results with minimal storage requirements and significantly less computational time than would be required with direct integration are obtained. Based on numerous test simulations, an error tolerance in the range of $10^{-3}-10^{-4}$ is found to be satisfactory for carrying out full PDF simulations of methane thermochlorination reactors. The results presented here demonstrate that the implementation of ISAT makes possible the hitherto formidable task of implementing detailed chemistry in CFD simulations of methane thermochlorination reactors.

1. Introduction

Chlorinated hydrocarbons occupy a unique and important place in the economy of the chemical industry. Indeed, they provide the principal routes by which chlorine reaches the heavy chemical market. Gas-phase thermochlorination of methane, widely used in the chemical industry since as early as 1923, yields all four chlorinated derivatives (i.e., methyl chloride, methylene dichloride, chloroform, and carbon tetrachloride) along with several other byproducts.[1] These chlorinated products have wide-ranging applications as industrial solvents, intermediates, and chemical products.[2] Chlorinated solvents, for example, are used in a variety of industrial applications due to their following unique properties: (1) ability to dissolve a wide range of organic substances, (2) moderate to extremely rapid evaporation rates, (3) low flammability, and (4) relative inertness to chemical reactivity. One such solvent, methylene dichloride, has found extensive applications in the manufacture of adhesives, aerosols, extraction solvents, industrial cleaning solvents, paint and coating solvents, and pharmaceuticals. Methyl chloride, on the other hand, is used exclusively to make silicone. In 1995, the production of methyl chloride was 483 000 metric tons as reported in *Chemical and Engineering News*.[3] The other two chlorinated derivatives of methane—chloroform and carbon tetrachloride—are used as chemical intermediates in the manufacture of chlorofluorocarbons (CFCs).

In a typical industrial methane thermal chlorination process, a chlorine−methane mixture and recycled chloromethanes are fed to a tubular reactor which is fully turbulent with high levels of mixing generated by the feed streams in the form of incoming jets. At a reactor temperature of 490−530 °C, all four chlorinated methane derivatives are produced along with several other byproducts. The detailed kinetic scheme employed in this work[4] involves three elements (H, C, Cl) and 38 chemical species (see Table 1) undergoing a total of 152 elementary reactions (Tables 2−6). The reaction is a classic example of the situation where the product distribution obtained depends on the conversion to which the reaction is taken. The relative amounts of different products can be changed by varying the reaction conditions.[1] Detailed modeling and simulation will help to understand the underlying chemistry and transport phenomena which can then be effectively used to explore reactor conditions that are beyond available experimental facilities. The modeling and accurate simulation of the performance of these reactors is particularly difficult as it involves the simulation of various physical processes and their interaction in turbulent reacting flows with complex chemical kinetics. The coupling between these processes is often the most complicated part to quantify and imposes severe restrictions on accurate simulation of the chemical reactor using computational fluid dynamics (CFD) because of the limitation of computational resources.[5]

Recently, CFD simulation of turbulent reacting flows, including detailed chemistry schemes, has received considerable attention due to the availability of faster computers, the development of new algorithms, and the establishment of elementary reaction schemes.[6−8] However, for the methane thermochlorination reaction a key problem remaining is the stiffness of the governing differential equations due to the wide range of chemical time scales. Therefore chemical reactor simulations often use a simplified model, either of the flow or of the chemistry (see ref 9 for a detailed discussion of the difficulties associated with kinetic model reduction).

* Author to whom correspondence should be addressed. E-mail: rofox@iastate.edu.

10.1021/ie990125g CCC: $18.00
Published on Web 10/01/1999

Table 1. List of Thirty-eight Chemical Species Appearing in Methane Thermochlorination Kinetic Scheme[a]

major species	HCl	Cl_2	CH_4	CH_3Cl
	CH_2Cl_2			
minor species	$CHCl_3$	CCl_4	$CHCl_2-CH_2Cl$	CH_2Cl-CH_2Cl
	CCl_3-CCl_3	CCl_3-CH_2Cl	CCl_3-CHCl_2	$CH_2=CH_2$
	t-CHCl=CHCl	*c*-CHCl=CHCl	$CHCl=CH_2$	$CCl_2=CHCl$
	$CHCl_2-CHCl_2$	$CCl_2=CH_2$		
ppm species	$CCl_2-CCl_2^{\bullet}$	CCl_3-CH_3	$Cl^{\bullet}$	$CH_3^{\bullet}$
	$CHCl_2^{\bullet}$	$CCl_3^{\bullet}$	$CH_2Cl-CH_2^{\bullet}$	$CH_2Cl-CCl_2^{\bullet}$
	$CH_2Cl-CHCl^{\bullet}$	$CH_2Cl-CH_2^{\bullet}$	$CHCl_2-CCl_2^{\bullet}$	$CCl_3-CCl_2^{\bullet}$
	$CCl_3-CHCl^{\bullet}$	*c*-CHCl=CCl	*t*-CHCl=CCl	$CH_3-CCl_2^{\bullet}$
	$CH_2Cl^{\bullet}$	$CHCl_2-CHCl^{\bullet}$	$CCl_3-CH_2^{\bullet}$	

[a] The superscript bullet denotes free-radical species.

Table 2. Twenty-one Unimolecular Decomposition Reactions

no.	reaction	A_n	E_n
1	$Cl_2 \rightleftharpoons 2Cl^{\bullet}$	0.115E+12	0.580E+5
2	$CH_3Cl \rightleftharpoons CH_3^{\bullet} + Cl^{\bullet}$	0.1E+17	0.844E+5
3	$CH_2Cl_2 \rightleftharpoons CH_2Cl^{\bullet} + Cl^{\bullet}$	0.1E+17	0.811E+5
4	$CHCl_2-CH_2Cl \rightleftharpoons CHCl_2^{\bullet} + CH_2Cl^{\bullet}$	0.1E+18	0.884E+5
5	$CH_2Cl-CH_2Cl \rightleftharpoons 2CH_2Cl^{\bullet}$	0.1E+18	0.901E+5
6	$CHCl_3 \rightleftharpoons CHCl_2^{\bullet} + Cl^{\bullet}$	0.1E+17	0.776E+5
7	$CHCl_2-CHCl_2 \rightleftharpoons 2CHCl_2^{\bullet}$	0.1E+18	0.824E+5
8	$CCl_3-CCl_3 \rightleftharpoons 2CCl_3^{\bullet}$	0.1E+18	0.714E+5
9	$CCl_3-CH_2Cl \rightleftharpoons CCl_3^{\bullet} + CH_2Cl^{\bullet}$	0.1E+18	0.827E+5
10	$CCl_3-CHCl_2 \rightleftharpoons CCl_3^{\bullet} + CHCl_2^{\bullet}$	0.1E+18	0.759E+5
11	$CCl_4 \rightleftharpoons CCl_3^{\bullet} + Cl^{\bullet}$	0.1E+17	0.709E+5
12	$CH_2Cl-CH_2^{\bullet} \rightleftharpoons CH_2=CH_2 + Cl^{\bullet}$	0.1E+15	0.203E+5
13	$CH_2Cl-CCl_2^{\bullet} \rightleftharpoons CCl_2=CH_2 + Cl^{\bullet}$	0.1E+15	0.259E+5
14	$CHCl_2-CHCl^{\bullet} \rightleftharpoons$ *t*-CHCl=CHCl + $Cl^{\bullet}$	0.1E+15	0.216E+5
15	$CHCl_2-CHCl^{\bullet} \rightleftharpoons$ *c*-CHCl=CHCl + $Cl^{\bullet}$	0.1E+15	0.211E+5
16	$CH_2Cl-CHCl^{\bullet} \rightleftharpoons CHCl=CH_2 + Cl^{\bullet}$	0.1E+15	0.229E+5
17	$CHCl_2-CH_2^{\bullet} \rightleftharpoons CHCl=CH_2 + Cl^{\bullet}$	0.1E+15	0.192E+5
18	$CHCl_2-CCl_2^{\bullet} \rightleftharpoons CCl_2=CHCl + Cl^{\bullet}$	0.1E+15	0.212E+5
19	$CCl_3-CCl_2^{\bullet} \rightleftharpoons CCl_2=CCl_2 + Cl^{\bullet}$	0.1E+15	0.194E+5
20	$CCl_3-CH_2^{\bullet} \rightleftharpoons CCl_2=CH_2 + Cl^{\bullet}$	0.1E+15	0.175E+5
21	$CCl_3-CHCl^{\bullet} \rightleftharpoons CCl_2=CHCl + Cl^{\bullet}$	0.1E+15	0.185E+5

Table 3. Twenty-six Metathesis Reactions

no.	reaction	A_n	E_n
1	*c*-CHCl=CHCl + $Cl^{\bullet} \rightleftharpoons$ *c*-CHCl=$CCl^{\bullet}$ + HCl	0.1E+14	0.196E+4
2	*t*-CHCl=CHCl + $Cl^{\bullet} \rightleftharpoons$ *t*-CHCl=$CCl^{\bullet}$ + HCl	0.1E+14	0.151E+4
3	$CH_3Cl + Cl^{\bullet} \rightleftharpoons CH_2Cl^{\bullet} + HCl$	0.1E+14	0.460E+3
4	$CH_3Cl + Cl^{\bullet} \rightleftharpoons CH_3^{\bullet} + Cl_2$	0.1E+15	0.256E+5
5	$CH_4 + Cl^{\bullet} \rightleftharpoons CH_3^{\bullet} + HCl$	0.1E+14	0.211E+4
6	$CH_4 + CH_2Cl^{\bullet} \rightleftharpoons CH_3^{\bullet} + CH_3Cl$	0.3E+12	0.158E+5
7	$CH_2Cl_2 + Cl^{\bullet} \rightleftharpoons CHCl_2^{\bullet} + HCl$	0.1E+14	0.460E+3
8	$CH_2Cl_2 + CH_3^{\bullet} \rightleftharpoons CHCl_2^{\bullet} + CH_4$	0.3E+12	0.110E+5
9	$CH_2Cl_2 + CH_2Cl^{\bullet} \rightleftharpoons CHCl_2^{\bullet} + CH_3Cl$	0.3E+12	0.110E+5
10	$CH_2Cl_2 + Cl^{\bullet} \rightleftharpoons CH_2Cl^{\bullet} + Cl_2$	0.1E+15	0.224E+5
11	$CH_2Cl_2 + CH_3^{\bullet} \rightleftharpoons CH_2Cl^{\bullet} + CH_3Cl$	0.3E+12	0.110E+5
12	$CHCl_2-CH_2Cl + Cl^{\bullet} \rightleftharpoons CHCl_2^{\bullet}-CHCl^{\bullet} + HCl$	0.1E+14	0.460E+3
13	$CHCl_2-CH_2Cl + Cl^{\bullet} \rightleftharpoons CH_2Cl-CCl_2^{\bullet} + HCl$	0.1E+14	0.460E+3
14	$CH_2Cl-CH_2Cl + Cl^{\bullet} \rightleftharpoons CH_2Cl-CHCl^{\bullet} + HCl$	0.1E+14	0.460E+3
15	$CHCl_3 + Cl^{\bullet} \rightleftharpoons CCl_3^{\bullet} + HCl$	0.1E+14	0.460E+3
16	$CHCl_3 + CH_3^{\bullet} \rightleftharpoons CCl_3^{\bullet} + CH_4$	0.3E+12	0.110E+5
17	$CHCl_3 + CH_2Cl^{\bullet} \rightleftharpoons CCl_3^{\bullet} + CH_3Cl$	0.3E+12	0.110E+5
18	$CHCl_3 + CHCl_2^{\bullet} \rightleftharpoons CCl_3^{\bullet} + CH_2Cl_2$	0.3E+12	0.110E+5
19	$CHCl_3 + Cl^{\bullet} \rightleftharpoons CHCl_2^{\bullet} + Cl_2$	0.1E+15	0.189E+5
20	$CHCl_3 + CH_3^{\bullet} \rightleftharpoons CHCl_2^{\bullet} + CH_3Cl$	0.3E+12	0.110E+5
21	$CHCl_3 + CH_2Cl^{\bullet} \rightleftharpoons CHCl_2^{\bullet} + CH_2Cl_2$	0.3E+12	0.110E+5
22	$CHCl_2-CHCl_2 + Cl^{\bullet} \rightleftharpoons CHCl_2-CCl_2^{\bullet} + HCl$	0.1E+14	0.460E+3
23	$CCl_4 + Cl^{\bullet} \rightleftharpoons CCl_3^{\bullet} + Cl_2$	0.1E+15	0.122E+5
24	$CCl_4 + CH_3^{\bullet} \rightleftharpoons CCl_3^{\bullet} + CH_3Cl$	0.3E+12	0.110E+5
25	$CCl_4 + CH_2Cl^{\bullet} \rightleftharpoons CCl_3^{\bullet} + CH_2Cl_2$	0.3E+12	0.110E+5
26	$CCl_4 + CHCl_2^{\bullet} \rightleftharpoons CCl_3^{\bullet} + CHCl_3$	0.3E+12	0.110E+5

These simplifications can be risky due to the strong interaction between the turbulent flow and the thermochlorination chemistry. Liu and Barkelew[10] appear to have been the first to attempt a full CFD simulation of an industrial methane thermochlorination reactor in order to study the dependence of the flow pattern and product yield on reactor geometry and operating conditions. However, due to the computational requirements, they had to limit their kinetic scheme to just three chemical reactions and six chemical species. Thus, although they were able to successfully compare their results for flow patterns with experimental data, they were unable to account for the minor species occurring in the reactor. Roekaerts[11] has approached the same problem using full probability density function (PDF) simulations with considerable success as far as the flow pattern is concerned. However, due to the computational expense, the chemical kinetic scheme was limited to just three reactions, which is far from what occurs in a real reactor. More recently, other authors have attempted CFD simulations of methane thermochlorination reactors.[12,13] In general, they have concluded that unless a detailed chemistry scheme is utilized, CFD does a poor job of predicting finite-rate chemistry effects, minor species formation, and local reaction extinction.

For the accurate prediction of minor species, full PDF methods need to be incorporated in a CFD simulation due to their ability to account for turbulence-chemistry interactions by treating complex reactions without any modeling assumptions.[5,14] In the computational implementation of full PDF methods, the fluid within the computational domain is represented by a large number of notional particles. The composition of each particle evolves according to a set of ordinary differential equations (ODEs). Typically, a two-dimensional simulation based on particle methods involves on the order of 10^6 particles evolving over 10^3 time steps. Consequently, the number of integrations of the stiff ODEs representing the chemical kinetics may be of the order of 1 billion. For example, on a SUN ULTRA 30 workstation using a standard numerical integration scheme, the 38-species mechanism for methane thermochlorination would require about 8 years of CPU time for a full PDF simulation, which is generally deemed to be prohibitively expensive. This duality of incorporating detailed chemistry for prediction of minor species on the one hand, and the computational expense of using full PDF methods on the other, has been a significant impediment for CFD modeling of methane thermochlorination reactors to research engineers in industry as well as academia. However the implementation of "smarter" in situ adaptive tabulation (ISAT) algorithms offers the promise of overcoming this roadblock by providing accurate results for complex chemical kinetic schemes with acceptable computational cost.[15]

In this study, we have implemented the ISAT algorithm[16] for methane thermochlorination chemistry and validated it using simulation results for a pairwise-mixing stirred reactor (PMSR) model. All the computations reported here have been performed on a SUN ULTRA 30 workstation. Conceptually, the PMSR model represents a single grid cell in a full PDF calculation

Table 4. Chaperon Reactions 1−40

no.	reaction	A_n	E_n
1	$CCl_2-CCl_2 + Cl_2 \rightleftharpoons CCl_3-CCl_2^{\bullet} + Cl^{\bullet}$	0.1E+14	0.399E+5
2	$CCl_2-CHCl + Cl_2 \rightleftharpoons CHCl_2-CCl_2^{\bullet} + Cl^{\bullet}$	0.1E+14	0.380E+5
3	$CCl_2-CHCl + Cl_2 \rightleftharpoons CCl_3-CHCl^{\bullet} + Cl^{\bullet}$	0.1E+14	0.408E+5
4	c-$CHCl=CHCl + Cl_2 \rightleftharpoons CHCl_2-CHCl^{\bullet} + Cl^{\bullet}$	0.1E+14	0.375E+5
5	t-$CHCl=CHCl + Cl_2 \rightleftharpoons CHCl_2-CHCl^{\bullet} + Cl^{\bullet}$	0.1E+14	0.374E+5
6	$CCl_2=CH_2 + Cl_2 \rightleftharpoons CH_2Cl-CCl_2^{\bullet} + Cl^{\bullet}$	0.1E+14	0.346E+5
7	$CCl_2=CH_2 + Cl_2 \rightleftharpoons CCl_3-CH_2^{\bullet} + Cl^{\bullet}$	0.1E+14	0.429E+5
8	$CHCl=CH_2 + Cl_2 \rightleftharpoons CH_2Cl-CHCl^{\bullet} + Cl^{\bullet}$	0.1E+14	0.373E+5
9	$CHCl=CH_2 + Cl_2 \rightleftharpoons CHCl_2-CH_2^{\bullet} + Cl^{\bullet}$	0.1E+14	0.410E+5
10	$CHCl=CH_2 + CH_2Cl-CH_2Cl \rightleftharpoons CHCl_2-CH_2^{\bullet} + CH_2Cl-CH_2^{\bullet}$	0.3E+15	0.664E+5
11	$CHCl=CH_2 + CHCl_2-CH_2Cl \rightleftharpoons CHCl_2-CH_2^{\bullet} + CHCl_2-CH_2^{\bullet}$	0.3E+15	0.647E+5
12	$CHCl=CH_2 + CCl_3-CH3 \rightleftharpoons CHCl_2-CH_2^{\bullet} + CH3-CCl_2^{\bullet}$	0.3E+15	0.567E+5
13	$CHCl=CH_2 + CCl_3-CH_2Cl \rightleftharpoons CHCl_2-CH_2^{\bullet} + CCl_3-CH_2^{\bullet}$	0.3E+15	0.614E+5
14	$CHCl=CH_2 + CCl_3-CH_2Cl \rightleftharpoons CHCl_2-CH_2^{\bullet} + CH_2Cl-CCl_2^{\bullet}$	0.3E+15	0.531E+5
15	$CHCl=CH_2 + CCl_3-CHCl_2 \rightleftharpoons CHCl_2-CH_2^{\bullet} + CCl_3-CHCl^{\bullet}$	0.3E+15	0.553E+5
16	$CHCl=CH_2 + CCl_3-CHCl_2 \rightleftharpoons CHCl_2-CH_2^{\bullet} + CHCl_2-CCl_2^{\bullet}$	0.3E+15	0.526E+5
17	$CHCl=CH_2 + CCl_3-CCl_3 \rightleftharpoons CHCl_2-CH_2^{\bullet} + CCl_3-CCl_2^{\bullet}$	0.3E+15	0.542E+5
18	$CHCl=CH_2 + CCl_4 \rightleftharpoons CHCl_2-CH_2^{\bullet} + CCl_3$	0.3E+15	0.527E+5
19	$CHCl=CH_2 + CHCl_2-CHCl_2 \rightleftharpoons CHCl_2-CH_2^{\bullet} + CHCl_2-CHCl^{\bullet}$	0.3E+15	0.568E+5
20	$CHCl=CH_2 + CH_2Cl-CH_2Cl \rightleftharpoons CH_2Cl-CHCl^{\bullet} + CH_2Cl-CH_2^{\bullet}$	0.3E+15	0.627E+5
21	$CHCl=CH_2 + CHCl_2-CH_2Cl \rightleftharpoons CH_2Cl-CHCl^{\bullet} + CHCl_2-CH_2^{\bullet}$	0.3E+15	0.610E+5
22	$CHCl=CH_2 + CHCl_2-CH_2Cl \rightleftharpoons CH_2Cl-CHCl^{\bullet} + CH_2Cl-CHCl^{\bullet}$	0.3E+15	0.573E+5
23	$CHCl=CH_2 + CCl_3-CH3 \rightleftharpoons CH_2Cl-CHCl^{\bullet} + CH3-CCl_2^{\bullet}$	0.3E+15	0.530E+5
24	$CHCl=CH_2 + CCl_3-CH_2Cl \rightleftharpoons CH_2Cl-CHCl^{\bullet} + CCl_3-CH_2^{\bullet}$	0.3E+15	0.577E+5
25	$CHCl=CH_2 + CCl_3-CH_2Cl \rightleftharpoons CH_2Cl-CHCl^{\bullet} + CH_2Cl-CCl_2^{\bullet}$	0.3E+15	0.494E+5
26	$CHCl=CH_2 + CCl_3-CHCl_2 \rightleftharpoons CH_2Cl-CHCl^{\bullet} + CCl_3-CHCl^{\bullet}$	0.3E+15	0.516E+5
27	$CHCl=CH_2 + CCl_3-CHCl_2 \rightleftharpoons CH_2Cl-CHCl^{\bullet} + CHCl_2-CCl_2^{\bullet}$	0.3E+15	0.489E+5
28	$CHCl=CH_2 + CCl_3-CCl_3 \rightleftharpoons CH_2Cl-CHCl^{\bullet} + CCl_3-CCl_2^{\bullet}$	0.3E+15	0.505E+5
29	$CHCl=CH_2 + CCl_4 \rightleftharpoons CH_2Cl-CHCl^{\bullet} + CCl_3^{\bullet}$	0.3E+15	0.490E+5
30	$CHCl=CH_2 + CHCl_2-CHCl_2 \rightleftharpoons CH_2Cl-CHCl^{\bullet} + CHCl_2-CHCl^{\bullet}$	0.3E+15	0.531E+5
31	$CCl_2=CH_2 + CH_2Cl-CH_2Cl \rightleftharpoons CCl_3-CH_2^{\bullet} + CH_2Cl-CH_2^{\bullet}$	0.3E+15	0.683E+5
32	$CCl_2=CH_2 + CHCl_2-CH_2Cl \rightleftharpoons CCl_3-CH_2^{\bullet} + CHCl_2-CH_2^{\bullet}$	0.3E+15	0.667E+5
33	$CCl_2=CH_2 + CHCl_2-CH_2Cl \rightleftharpoons CCl_3-CH_2^{\bullet} + CH_2Cl-CHCl^{\bullet}$	0.3E+15	0.630E+5
34	$CCl_2=CH_2 + CCl_3-CH3 \rightleftharpoons CCl_3-CH_2^{\bullet} + CH3-CCl_2^{\bullet}$	0.3E+15	0.586E+5
35	$CCl_2=CH_2 + CCl_3-CH_2Cl \rightleftharpoons CCl_3-CH_2^{\bullet} + CCl_3-CH_2^{\bullet}$	0.3E+15	0.634E+5
36	$CCl_2=CH_2 + CCl_3-CHCl_2 \rightleftharpoons CCl_3-CH_2^{\bullet} + CCl_3-CHCl^{\bullet}$	0.3E+15	0.573E+5
37	$CCl_2=CH_2 + CCl_3-CHCl_2 \rightleftharpoons CCl_3-CH_2^{\bullet} + CHCl_2-CCl_2^{\bullet}$	0.3E+15	0.545E+5
38	$CCl_2=CH_2 + CCl_3-CCl_3 \rightleftharpoons CCl_3-CH_2^{\bullet} + CCl_3-CCl_2^{\bullet}$	0.3E+15	0.561E+5
39	$CCl_2=CH_2 + CCl_4 \rightleftharpoons CCl_3-CH_2^{\bullet} + CCl_3$	0.3E+15	0.547E+5
40	$CCl_2=CH_2 + CHCl_2-CHCl_2 \rightleftharpoons CCl_3-CH_2^{\bullet} + CHCl_2-CHCl^{\bullet}$	0.3E+15	0.588E+5

and thus provides an accurate estimate of the computational gains that can be expected when employing the ISAT algorithm in actual reactor simulations. Physically, the PMSR reactor represents a perfectly macromixed, poorly micromixed stirred-tank reactor. As the micromixing time, τ_{mix}, approaches zero, the PMSR model reduces to a perfectly mixed *adiabatic* CSTR. Thus, from a chemical reaction engineering standpoint, the results presented in this work for various values of τ_{mix} give an indication of how sensitive the methane thermochlorination reaction is to micromixing. However, since the turbulent flow field inside of a plant-scale reactor will be far from well macromixed, a detailed PDF study of such a reactor (which will require ISAT!) will be needed to completely understand the effects of turbulent mixing on the reactor performance. Hence, in this work, we limit our consideration to demonstrating that the methane thermochlorination kinetic scheme can be successfully treated using ISAT.

The remainder of the paper has been organized as follows. In section 2, the detailed kinetic scheme for methane thermochlorination involving 38 chemical species and 152 elementary reactions is introduced. In section 3, the formulation of the PMSR model is reviewed. In section 4, an overview of the ISAT algorithm and its implementation for methane thermochlorination is presented. A detailed error analysis comparing ISAT results to direct integration (DI) results is given in section 5. Simulation results for methane thermochlorination in the PMSR model are discussed in section 6, and conclusions are drawn in section 7.

2. Methane Thermochlorination Kinetics

Methane can be chlorinated thermally, photochemically, or catalytically.[1,2] However, from a reactor engineering standpoint, thermochlorination is the most difficult method, involving a free-radical chain reaction which is limited by the presence of oxygen and other free-radical inhibitors. The full kinetic scheme employed in this work[4] involves three elements (H, C, Cl) and 38 chemical species (see Table 1) undergoing a total of 152 elementary reactions (Tables 2−6). Thus the complexity of the mechanism adequately justifies our selection of this kinetic scheme for testing the ISAT algorithm. Indeed, due to the large number of chemical species, the only other method that can treat this scheme is direct numerical integration (DI). However, we shall see that it too must be ruled out for all but the simplest reactor models due to its large computational cost.

The detailed kinetic scheme for methane thermochlorination is given in Tables 2−6 where the preexponential factor, A_n, and the activation energy, E_n, have units of 1/s and cal/mol, respectively, and the forward rate constants have the form

$$k_n^{\mathrm{f}} = A_n \exp\left(-\frac{E_n}{R_c T}\right) \tag{1}$$

The first step in the kinetic scheme is the thermal dissociation of the chlorine molecules (reaction 1 in Table 2). The chlorine atoms then react with methane to form hydrogen chloride and a methyl radical (reaction 5 in Table 3). The methyl radical in turn reacts with a chlorine molecule to form methyl chloride and another

Table 5. Chaperon Reactions 41−80

no.	reaction	A_n	E_n
41	$CCl_2{=}CH_2 + CH_2Cl{-}CH_2Cl \rightleftharpoons CH_2Cl{-}CCl_2^{\bullet} + CH_2Cl{-}CH_2^{\bullet}$	0.3E+15	0.599E+5
42	$CCl_2{=}CH_2 + CHCl_2{-}CH_2Cl \rightleftharpoons CH_2Cl{-}CCl_2^{\bullet} + CHCl_2{-}CH_2^{\bullet}$	0.3E+15	0.583E+5
43	$CCl_2{=}CH_2 + CHCl_2{-}CH_2Cl \rightleftharpoons CH_2Cl{-}CCl_2^{\bullet} + CH_2Cl{-}CHCl^{\bullet}$	0.3E+15	0.546E+5
44	$CCl_2{=}CH_2 + CCl_3{-}CH3 \rightleftharpoons CH_2Cl{-}CCl_2^{\bullet} + CH3{-}CCl_2^{\bullet}$	0.3E+15	0.502E+5
45	$CCl_2{=}CH_2 + CCl_3{-}CH_2Cl \rightleftharpoons CH_2Cl{-}CCl_2^{\bullet} + CCl_3{-}CH_2^{\bullet}$	0.3E+15	0.550E+5
46	$CCl_2{=}CH_2 + CCl_3{-}CH_2Cl \rightleftharpoons CH_2Cl{-}CCl_2^{\bullet} + CH_2Cl{-}CCl_2^{\bullet}$	0.3E+15	0.466E+5
47	$CCl_2{=}CH_2 + CCl_3{-}CHCl_2 \rightleftharpoons CH_2Cl{-}CCl_2^{\bullet} + CCl_3{-}CHCl^{\bullet}$	0.3E+15	0.489E+5
48	$CCl_2{=}CH_2 + CCl_3{-}CHCl_2 \rightleftharpoons CH_2Cl{-}CCl_2^{\bullet} + CHCl_2{-}CCl_2^{\bullet}$	0.3E+15	0.461E+5
49	$CCl_2{=}CH_2 + CCl_3{-}CCl_3 \rightleftharpoons CH_2Cl{-}CCl_2^{\bullet} + CCl_3{-}CCl_2^{\bullet}$	0.3E+15	0.477E+5
50	$CCl_2{=}CH_2 + CCl_4 \rightleftharpoons CH_2Cl{-}CCl_2^{\bullet} + CCl_3^{\bullet}$	0.3E+15	0.463E+5
51	$CCl_2{=}CH_2 + CHCl_2{-}CHCl_2 \rightleftharpoons CH_2Cl{-}CCl_2^{\bullet} + CHCl_2{-}CHCl^{\bullet}$	0.3E+15	0.504E+5
52	$t\text{-}CHCl{=}CHCl + CH_2Cl{-}CH_2Cl \rightleftharpoons CHCl_2{-}CHCl^{\bullet} + CH_2Cl{-}CH_2^{\bullet}$	0.3E+15	0.628E+5
53	$t\text{-}CHCl{=}CHCl + CHCl_2{-}CH_2Cl \rightleftharpoons CHCl_2{-}CHCl^{\bullet} + CHCl_2{-}CH_2^{\bullet}$	0.3E+15	0.611E+5
54	$t\text{-}CHCl{=}CHCl + CHCl_2{-}CH_2Cl \rightleftharpoons CHCl_2{-}CHCl^{\bullet} + CH_2Cl{-}CHCl^{\bullet}$	0.3E+15	0.574E+5
55	$t\text{-}CHCl{=}CHCl + CCl_3{-}CH3 \rightleftharpoons CHCl_2{-}CHCl^{\bullet} + CH3{-}CCl_2^{\bullet}$	0.3E+15	0.530E+5
56	$t\text{-}CHCl{=}CHCl + CCl_3{-}CH_2Cl \rightleftharpoons CHCl_2{-}CHCl^{\bullet} + CCl_3{-}CH_2^{\bullet}$	0.3E+15	0.578E+5
57	$t\text{-}CHCl{=}CHCl + CCl_3{-}CH_2Cl \rightleftharpoons CHCl_2{-}CHCl^{\bullet} + CH_2Cl{-}CCl_2^{\bullet}$	0.3E+15	0.494E+5
58	$t\text{-}CHCl{=}CHCl + CCl_3{-}CHCl_2 \rightleftharpoons CHCl_2{-}CHCl^{\bullet} + CCl_3{-}CHCl^{\bullet}$	0.3E+15	0.517E+5
59	$t\text{-}CHCl{=}CHCl + CCl_3{-}CHCl_2 \rightleftharpoons CHCl_2{-}CHCl^{\bullet} + CHCl_2{-}CCl_2^{\bullet}$	0.3E+15	0.489E+5
60	$t\text{-}CHCl{=}CHCl + CCl_3{-}CCl_3 \rightleftharpoons CHCl_2{-}CHCl^{\bullet} + CCl_3{-}CCl_2^{\bullet}$	0.3E+15	0.505E+5
61	$t\text{-}CHCl{=}CHCl + CCl_4 \rightleftharpoons CHCl_2{-}CHCl^{\bullet} + CCl_3^{\bullet}$	0.3E+15	0.491E+5
62	$t\text{-}CHCl{=}CHCl + CHCl_2{-}CHCl_2 \rightleftharpoons CHCl_2{-}CHCl^{\bullet} + CHCl_2{-}CHCl^{\bullet}$	0.3E+15	0.532E+5
63	$c\text{-}CHCl{=}CHCl + CH_2Cl{-}CH_2Cl \rightleftharpoons CHCl_2{-}CHCl^{\bullet} + CH_2Cl{-}CH_2^{\bullet}$	0.3E+15	0.629E+5
64	$c\text{-}CHCl{=}CHCl + CHCl_2{-}CH_2Cl \rightleftharpoons CHCl_2{-}CHCl^{\bullet} + CHCl_2{-}CH_2^{\bullet}$	0.3E+15	0.612E+5
65	$c\text{-}CHCl{=}CHCl + CHCl_2{-}CH_2Cl \rightleftharpoons CHCl_2{-}CHCl^{\bullet} + CH_2Cl{-}CHCl^{\bullet}$	0.3E+15	0.575E+5
66	$c\text{-}CHCl{=}CHCl + CCl_3{-}CH3 \rightleftharpoons CHCl_2{-}CHCl^{\bullet} + CH3{-}CCl_2^{\bullet}$	0.3E+15	0.531E+5
67	$c\text{-}CHCl{=}CHCl + CCl_3{-}CH_2Cl \rightleftharpoons CHCl_2{-}CHCl^{\bullet} + CCl_3{-}CH_2^{\bullet}$	0.3E+15	0.579E+5
68	$c\text{-}CHCl{=}CHCl + CCl_3{-}CH_2Cl \rightleftharpoons CHCl_2{-}CHCl^{\bullet} + CH_2Cl{-}CCl_2^{\bullet}$	0.3E+15	0.495E+5
69	$c\text{-}CHCl{=}CHCl + CCl_3{-}CHCl_2 \rightleftharpoons CHCl_2{-}CHCl^{\bullet} + CCl_3{-}CHCl^{\bullet}$	0.3E+15	0.518E+5
70	$c\text{-}CHCl{=}CHCl + CCl_3{-}CHCl_2 \rightleftharpoons CHCl_2{-}CHCl^{\bullet} + CHCl_2{-}CCl_2^{\bullet}$	0.3E+15	0.490E+5
71	$c\text{-}CHCl{=}CHCl + CCl_3{-}CCl_3 \rightleftharpoons CHCl_2{-}CHCl^{\bullet} + CCl_3{-}CCl_2^{\bullet}$	0.3E+15	0.506E+5
72	$c\text{-}CHCl{=}CHCl + CCl_4 \rightleftharpoons CHCl_2{-}CHCl^{\bullet} + CCl_3^{\bullet}$	0.3E+15	0.492E+5
73	$c\text{-}CHCl{=}CHCl + CHCl_2{-}CHCl_2 \rightleftharpoons CHCl_2{-}CHCl^{\bullet} + CHCl_2{-}CHCl^{\bullet}$	0.3E+15	0.533E+5
74	$CCl_2{=}CHCl + CH_2Cl{-}CH_2Cl \rightleftharpoons CCl_3{-}CHCl^{\bullet} + CH_2Cl{-}CH_2^{\bullet}$	0.3E+15	0.661E+5
75	$CCl_2{=}CHCl + CHCl_2{-}CH_2Cl \rightleftharpoons CCl_3{-}CHCl^{\bullet} + CHCl_2{-}CH_2^{\bullet}$	0.3E+15	0.645E+5
76	$CCl_2{=}CHCl + CHCl_2{-}CH_2Cl \rightleftharpoons CCl_3{-}CHCl^{\bullet} + CH_2Cl{-}CHCl^{\bullet}$	0.3E+15	0.608E+5
77	$CCl_2{=}CHCl + CCl_3{-}CH3 \rightleftharpoons CCl_3{-}CHCl^{\bullet} + CH3{-}CCl_2^{\bullet}$	0.3E+15	0.564E+5
78	$CCl_2{=}CHCl + CCl_3{-}CH_2Cl \rightleftharpoons CCl_3{-}CHCl^{\bullet} + CCl_3{-}CH_2^{\bullet}$	0.3E+15	0.612E+5
79	$CCl_2{=}CHCl + CCl_3{-}CH_2Cl \rightleftharpoons CCl_3{-}CHCl^{\bullet} + CH_2Cl{-}CCl_2^{\bullet}$	0.3E+15	0.528E+5
80	$CCl_2{=}CHCl + CCl_3{-}CHCl_2 \rightleftharpoons CCl_3{-}CHCl^{\bullet} + CCl_3{-}CHCl^{\bullet}$	0.3E+15	0.551E+5

Table 6. Chaperon Reactions 81−105

no.	reaction	A_n	E_n
81	$CCl_2{=}CHCl + CCl_3{-}CCl_3 \rightleftharpoons CCl_3{-}CHCl^{\bullet} + CCl_3{-}CCl_2^{\bullet}$	0.3E+15	0.539E+5
82	$CCl_2{=}CHCl + CCl_4 \rightleftharpoons CCl_3{-}CHCl^{\bullet} + CCl_3^{\bullet}$	0.3E+15	0.525E+5
83	$CCl_2{=}CHCl + CHCl_2{-}CHCl_2 \rightleftharpoons CCl_3{-}CHCl^{\bullet} + CHCl_2{-}CHCl^{\bullet}$	0.3E+15	0.566E+5
84	$CCl_2{=}CHCl + CH_2Cl{-}CH_2Cl \rightleftharpoons CHCl_2{-}CCl_2^{\bullet} + CH_2Cl{-}CH_2^{\bullet}$	0.3E+15	0.634E+5
85	$CCl_2{=}CHCl + CHCl_2{-}CH_2Cl \rightleftharpoons CHCl_2{-}CCl_2^{\bullet} + CHCl_2{-}CH_2^{\bullet}$	0.3E+15	0.617E+5
86	$CCl_2{=}CHCl + CHCl_2{-}CH_2Cl \rightleftharpoons CHCl_2{-}CCl_2^{\bullet} + CH_2Cl{-}CHCl^{\bullet}$	0.3E+15	0.580E+5
87	$CCl_2{=}CHCl + CCl_3{-}CH3 \rightleftharpoons CHCl_2{-}CCl_2^{\bullet} + CH3{-}CCl_2^{\bullet}$	0.3E+15	0.536E+5
88	$CCl_2{=}CHCl + CCl_3{-}CH_2Cl \rightleftharpoons CHCl_2{-}CCl_2^{\bullet} + CCl_3{-}CH_2^{\bullet}$	0.3E+15	0.584E+5
89	$CCl_2{=}CHCl + CCl_3{-}CH_2Cl \rightleftharpoons CHCl_2{-}CCl_2^{\bullet} + CH_2Cl{-}CCl_2^{\bullet}$	0.3E+15	0.500E+5
90	$CCl_2{=}CHCl + CCl_3{-}CHCl_2 \rightleftharpoons CHCl_2{-}CCl_2^{\bullet} + CCl_3{-}CHCl^{\bullet}$	0.3E+15	0.523E+5
91	$CCl_2{=}CHCl + CCl_3{-}CHCl_2 \rightleftharpoons CHCl_2{-}CCl_2^{\bullet} + CHCl_2{-}CCl_2^{\bullet}$	0.3E+15	0.495E+5
92	$CCl_2{=}CHCl + CCl_3{-}CCl_3 \rightleftharpoons CHCl_2{-}CCl_2^{\bullet} + CCl_3{-}CCl_2^{\bullet}$	0.3E+15	0.512E+5
93	$CCl_2{=}CHCl + CCl_4 \rightleftharpoons CHCl_2{-}CCl_2^{\bullet} + CCl_3^{\bullet}$	0.3E+15	0.497E+5
94	$CCl_2{=}CHCl + CHCl_2{-}CHCl_2 \rightleftharpoons CHCl_2{-}CCl_2^{\bullet} + CHCl_2{-}CHCl^{\bullet}$	0.3E+15	0.538E+5
95	$CCl_2{=}CCl_2 + CH_2Cl{-}CH_2Cl \rightleftharpoons CCl_3{-}CCl_2^{\bullet} + CH_2Cl{-}CH_2^{\bullet}$	0.3E+15	0.652E+5
96	$CCl_2{=}CCl_2 + CHCl_2{-}CH_2Cl \rightleftharpoons CCl_3{-}CCl_2^{\bullet} + CHCl_2{-}CH_2^{\bullet}$	0.3E+15	0.636E+5
97	$CCl_2{=}CCl_2 + CHCl_2{-}CH_2Cl \rightleftharpoons CCl_3{-}CCl_2^{\bullet} + CH_2Cl{-}CHCl^{\bullet}$	0.3E+15	0.599E+5
98	$CCl_2{=}CCl_2 + CCl_3{-}CH3 \rightleftharpoons CCl_3{-}CCl_2^{\bullet} + CH3{-}CCl_2^{\bullet}$	0.3E+15	0.555E+5
99	$CCl_2{=}CCl_2 + CCl_3{-}CH_2Cl \rightleftharpoons CCl_3{-}CCl_2^{\bullet} + CCl_3{-}CH_2^{\bullet}$	0.3E+15	0.603E+5
100	$CCl_2{=}CCl_2 + CCl_3{-}CH_2Cl \rightleftharpoons CCl_3{-}CCl_2^{\bullet} + CH_2Cl{-}CCl_2^{\bullet}$	0.3E+15	0.519E+5
101	$CCl_2{=}CCl_2 + CCl_3{-}CHCl_2 \rightleftharpoons CCl_3{-}CCl_2^{\bullet} + CCl_3{-}CHCl^{\bullet}$	0.3E+15	0.542E+5
102	$CCl_2{=}CCl_2 + CCl_3{-}CHCl_2 \rightleftharpoons CCl_3{-}CCl_2^{\bullet} + CHCl_2{-}CCl_2^{\bullet}$	0.3E+15	0.514E+5
103	$CCl_2{=}CCl_2 + CCl_3{-}CCl_3 \rightleftharpoons CCl_3{-}CCl_2^{\bullet} + CCl_3{-}CCl_2^{\bullet}$	0.3E+15	0.530E+5
104	$CCl_2{=}CCl_2 + CCl_4 \rightleftharpoons CCl_3{-}CCl_2^{\bullet} + CCl_3^{\bullet}$	0.3E+15	0.516E+5
105	$CCl_2{=}CCl_2 + CHCl_2{-}CHCl_2 \rightleftharpoons CCl_3{-}CCl_2^{\bullet} + CHCl_2{-}CHCl^{\bullet}$	0.3E+15	0.557E+5

chlorine atom (reaction 4 in Table 3) that can propagate the reaction and result in a large number of other chlorinated species (Tables 3−6). Chain termination may proceed in several ways due to the combination of any pair of free radicals (reactions 1−11 in Table 2 and Tables 4−6). As stated earlier, the conversion of methane is controlled by the ratio of chlorine to methane used, chlorine being completely consumed under process conditions. Operation at low conversion favors the production of less highly chlorinated products and high conversion the more highly chlorinated products. Thus it is not possible to operate the process so as to obtain only methyl chloride, since this is much more readily attacked by chlorine than methane itself. (This is attributed to the resonance stabilization of the incipient chloromethyl radical in the hydrogen abstraction stage, which is presumed to lead to an increased ease of abstraction of the H atom compared with the abstraction from methane.[1]) However, within this limitation, there is considerable flexibility, and the process can be operated to give mixtures of methyl chloride, methylene chloride, and chloroform, all four products, or carbon tetrachloride alone.

In a CFD simulation of methane thermochlorination, a transport equation of the form

$$\frac{\partial \phi}{\partial t} + \frac{\partial}{\partial x_i}[u_i \phi] = \frac{\partial}{\partial x_i}\left(D \frac{\partial \phi}{\partial x_i}\right) + \mathbf{S}(\phi) \tag{2}$$

will be required for each of the 38 chemical species and for the enthalpy. The resulting 39-component composition vector is denoted by $\phi(\mathbf{x},t)$. Using a fractional time-stepping algorithm to solve the transport equation, the chemical source term $\mathbf{S}(\phi)$ can be isolated from the convection and diffusion terms.[17] The chemical source term is formulated in terms of the elementary reactions. Representing the latter in terms of chemical species A_i and stoichiometric coefficients ν^{f}_{in} and ν^{r}_{in} by

$$\sum_{i=1}^{38} \nu^{f}_{in} A_i \underset{k^{r}_{n}}{\overset{k^{f}_{n}}{\rightleftharpoons}} \sum_{i=1}^{38} \nu^{f}_{n} A_i, \quad n = 1, ..., 152 \tag{3}$$

the chemical source for the jth chemical species can be expressed as

$$S_j(\phi) = \sum_{n=1}^{152} (\nu^{r}_{jn} - \nu^{f}_{jn})[k^{f}_{n}(T) \prod_{i=1}^{38} \phi_i^{\nu^{f}_{in}} - k^{r}_{n}(T) \prod_{i=1}^{38} \phi_i^{\nu^{r}_{in}}], \quad j = 1, ..., 38 \tag{4}$$

and the enthalpy term can be expressed as

$$S_{39}(\phi) = -\sum_{j=1}^{38} h_j(T)\, S_j(\phi) \tag{5}$$

where h_j is the specific enthalpy of the jth chemical species.

In this work, FORTRAN subroutines from Chemkin-II[18] have been used to generate the chemical source term and thermodynamic data using the detailed kinetic scheme given in Tables 2−6. The Chemkin-II input files for the kinetic scheme and the thermodynamic data are available upon request.

3. Pairwise Mixing Stirred Reactor

Because it generates a relatively large region in composition space as compared to other simple models,[15,19] the PMSR model was selected for testing the ISAT algorithm for methane thermochlorination. Moreover, the performance statistics and numerical difficulties experienced with the PMSR model should adequately reflect those expected with full PDF simulations. Thus the results obtained in these tests will be sufficient for optimizing the parameters in ISAT to minimize the computational time for subsequent incorporation in full PDF simulations. In addition, since the PMSR model represents a poorly micromixed adiabatic CSTR, the simulation results will be indicative of reactor performance under conditions of perfect macromixing.

At any time t, the PMSR model consists of an even number N of particles, the ith particle having composition $\phi^{(i)}(t)$. The PMSR model is simulated numerically by first assigning initial conditions to all particles present in the reactor at $t = 0$ and then advancing in discrete time steps until a statistically stationary state is attained. With δt being the specified fractional time step, at the discrete times $k\,\delta t$ events corresponding to outflow, inflow, and pairing can occur which will cause $\phi^{(i)}(t)$ to change discontinuously. Between these discrete times, the composition evolves by mixing and reaction fractional steps. This is analogous to full PDF methods wherein fractional time stepping is used to handle chemistry and transport processes separately.[5,17]

Table 7. Parameters Used in the PMSR Simulations

number of particles, N	100
time step, δt	0.07 s
number of time steps, N_{step}	1000
residence time, τ_{res}	7 s
mixing time scale, τ_{mix}	0.7 s
pairing time scale, τ_{pair}	0.7 s

In the PMSR model, the particles are arranged in pairs; i.e., particles 1 and 2, 3 and 4, ..., $N - 1$ and N are partners. The mixing fractional time step consists of a pair (e.g., p and q) evolving by a simple first-order linear model:

$$\frac{d\phi^{(p)}}{dt} = -\frac{1}{\tau_{mix}}(\phi^{(p)} - \phi^{(q)}) \tag{6}$$

$$\frac{d\phi^{(q)}}{dt} = -\frac{1}{\tau_{mix}}(\phi^{(q)} - \phi^{(p)}) \tag{7}$$

where τ_{mix} is the micromixing time scale. Note that because τ_{mix} is assumed to be constant over the fractional time step, these equations can be solved analytically and thus add little to the total computational cost of the simulation.

During the reaction fractional time step, each particle evolves according to the chemical source term:

$$\frac{d\phi^{(i)}}{dt} = \mathbf{S}(\phi^{(i)}) \tag{8}$$

where $\mathbf{S}(\phi^{(i)})$ is given by eq 4. The complexity of the chemical source term and, more importantly, the wide range of chemical time scales contained in the chemical rate expressions make the numerical solution of eq 8 quite costly relative to other terms in the model. In general, an initial-value solver for systems of stiff ODEs will be required to find $\phi^{(i)}(t + \delta t)$ given $\phi^{(i)}(t)$ [i.e., direct integration (DI)]. However, even with a state-of-the-art stiff ODE solver, the computational cost for updating the composition vector for each particle over many time steps will be prohibitive. The ISAT algorithm described in the next section attempts to overcome this difficulty by replacing DI with multilinear interpolation.

The other physical processes represented in the PMSR model are inflow and outflow to/from the reactor and reassignment of particle pairs. (The latter is required to ensure that mixing can take place between all particles in the reactor.) With τ_{res} being the specified residence time, inflow and outflow consist of selecting $N\,\delta t/(2\tau_{res})$ particle pairs at random and replacing their compositions with the inflow compositions which are drawn from a specified distribution (i.e., based on the relative flow rates of the two inlet feed streams and their chemical compositions). With τ_{pair} being the specified pairing time scale, $N\,\delta t(2\tau_{pair})$ particle pairs (other than inflowing particles) are randomly selected for pairing. These particles and the inflowing particles are then randomly shuffled so that (most likely) they change partners.

The values of the various parameters used in the tests are listed in Table 7. There are two inflowing streams to the reactor. Stream 1 contains 25% Cl_2, 50% CH_4, and 25% CH_3Cl (volume fraction) at 333 K, and stream

2 contains an equilibrium mixture of 25% Cl_2, 50% CH_4, and 25% CH_3Cl (volume fraction) at 333 K. The mass flow rates of these streams are in the ratio 0.25:1. Both streams are at a pressure of 2.38 atm. Initially ($t = 0$) all particle compositions in the reactor are set to the composition of stream 1. The selection of these initial and boundary conditions is in conjunction with an industrial test case, being studied elsewhere.[13] The tests described here have also been applied to other inlet conditions, and the results are in line with the general conclusions of this paper. The simulation parameters thus remain unchanged in all the tests reported (unless noted otherwise).

4. In Situ Adaptive Tabulation

As discussed earlier, the algorithm which is used to solve eq 8 will have a strong effect on numerical convergence and computational efficiency of the flow simulation. At each fractional time step, the chemical composition for all particles must be updated according to the chemical source term. This process can be represented mathematically by a nonlinear reaction mapping $\mathbf{R}(\phi)$:

$$\phi^{(i)}(t) \xrightarrow{\mathbf{R}} \phi^{(i)}(t + \delta t) \tag{9}$$

which maps the initial composition vector $\phi^{(i)}(t)$ to a new composition vector $\phi^{(i)}(t + \delta t)$. (Note that the reaction mapping is an implicit function of the time step δt.) The straightforward approach for finding the reaction mapping is to integrate the chemical source term numerically using a stiff ODE solver (i.e., DI). However, due to the wide range in the chemical time scales, this process is relatively expensive as compared to other operations. For the PMSR test case, 100 particles are used and the solution is advanced for 1000 time steps. Consequently, the reaction mapping must be found 10^5 times, which is computationally prohibitive using DI. For full PDF methods about 10^6 particles are used to simulate the flow field, and thus the reaction mapping would need to be found up to 10^9 times. Obviously, such a computation will only be tractable if a method many times more efficient than DI is employed.

To circumvent the computational cost of DI, two strategies can be used: simplified kinetics which neglect minor species[9] and chemical look-up tables.[5] For methane thermochlorination, the first is ruled out since the prediction of minor species is a prime objective. Likewise, due to memory storage requirements, traditional a priori chemical look-up tables are limited to kinetic schemes with at most five to six reactants. However, the application of in situ, *adaptive* tabulation (ISAT) overcomes the barriers associated with traditional look-up tables. In this work, the ISAT algorithm proposed by Pope[15] is shown to provide sufficiently accurate results with minimum computational effort for the 38-species methane thermochlorination kinetic scheme.

The efficiency of ISAT arises from its unique feature to take advantage of the compactness of the accessed region in composition space. (For the methane thermochlorination kinetic scheme, the composition space is the 39-dimensional vector space containing the composition vector ϕ.) The accessed region can be defined to be the set of all the composition vectors generated in a given simulation (i.e., with fixed initial and boundary conditions). In practice, the accessed region is often a very small subset of the realizable region where the latter is defined to be the subset of composition space containing all points which satisfy the constraints imposed by conservation of mass, conservation of enthalpy, and the stoichiometry of the kinetic scheme (e.g., conservation of elements). Thus, for a particular set of initial and boundary conditions, ISAT constructs a relatively small look-up table, covering only the accessed region. (In contrast, because the accessed region is unknown a priori, traditional tabulation schemes must cover the entire realizable region.) Nevertheless, because the size and location of the accessed region will vary from one flow simulation to another, the look-up table must be constructed as the calculation proceeds (i.e., in situ). We now give a brief overview of the ISAT algorithm, the details of which can be found elsewhere.[15]

The basic idea behind ISAT is to integrate the chemical source term directly using DI, and then to store not only the reaction mapping but also sensitivity information in a binary tree data structure for later use. For subsequent calculations, for points within a small distance of the previously tabulated points, DI is avoided by estimating the reaction mapping using multilinear interpolation. However, any reaction mapping that cannot be interpolated with sufficient accuracy is generated by DI and stored in the table. These essential ideas and ingredients of the ISAT approach are depicted in Figure 1 and summarized as follows:

1. A splitting scheme is employed so that the problem is reduced to determining the reaction mapping $\mathbf{R}(\phi)$, which is the solution to eq 8 after a time δt from the initial condition ϕ. (Note that because the right-hand side of eq 8 does not depend explicitly on t, the reaction mapping depends only on the initial conditions and the time increment.)

2. A table is built in situ (i.e., as the reacting flow calculation is performed) so that only the accessed region of the composition space is tabulated. (Thus, at the first time step, the table is empty.)

3. A table entry (or record) consists of (i) a reference composition vector ϕ^0, (ii) the reaction mapping evaluated at the reference composition vector $\mathbf{R}(\phi^0)$, (iii) the Jacobian matrix for the reaction mapping evaluated at the reference composition vector $\mathbf{A}(\phi^0)$, and (iv) information needed to define the ellipsoid of accuracy (EOA) discussed below. The reaction mapping and its Jacobian can then be used to obtain a linear approximation to the reaction mapping evaluated at a "nearby" query composition ϕ^q:

$$\mathbf{R}(\phi^q) \approx \mathbf{R}(\phi^0) + \mathbf{A}(\phi^0)(\phi^q - \phi^0) \tag{10}$$

The EOA is an ellipsoidal region, centered at ϕ^0, within which the linear approximation is known to be accurate, i.e., if $\phi^q \in$ EOA, then eq 10 approximates $\mathbf{R}(\phi^q)$ within a user-specified error tolerance. (Note that the EOA is an implicit function of ϕ^0.)

4. The EOA is defined in terms of the singular values of the Jacobian matrix and a user-specified error tolerance ϵ_{tol}. The mapping error ϵ is defined in terms of a weighted norm of the difference between the true value of $\mathbf{R}(\phi^q)$ and the right-hand side of eq 10. However, the definition of EOA in terms of the singular values may be overly conservative; i.e., query points are encountered for which the linear estimate is within the region of accuracy ($\epsilon < \epsilon_{tol}$), but yet fall outside of the EOA. A *growth process* is thus employed to expand the EOA into a hyper-ellipsoid of minimum volume that contains both the original EOA and the query point. Because it

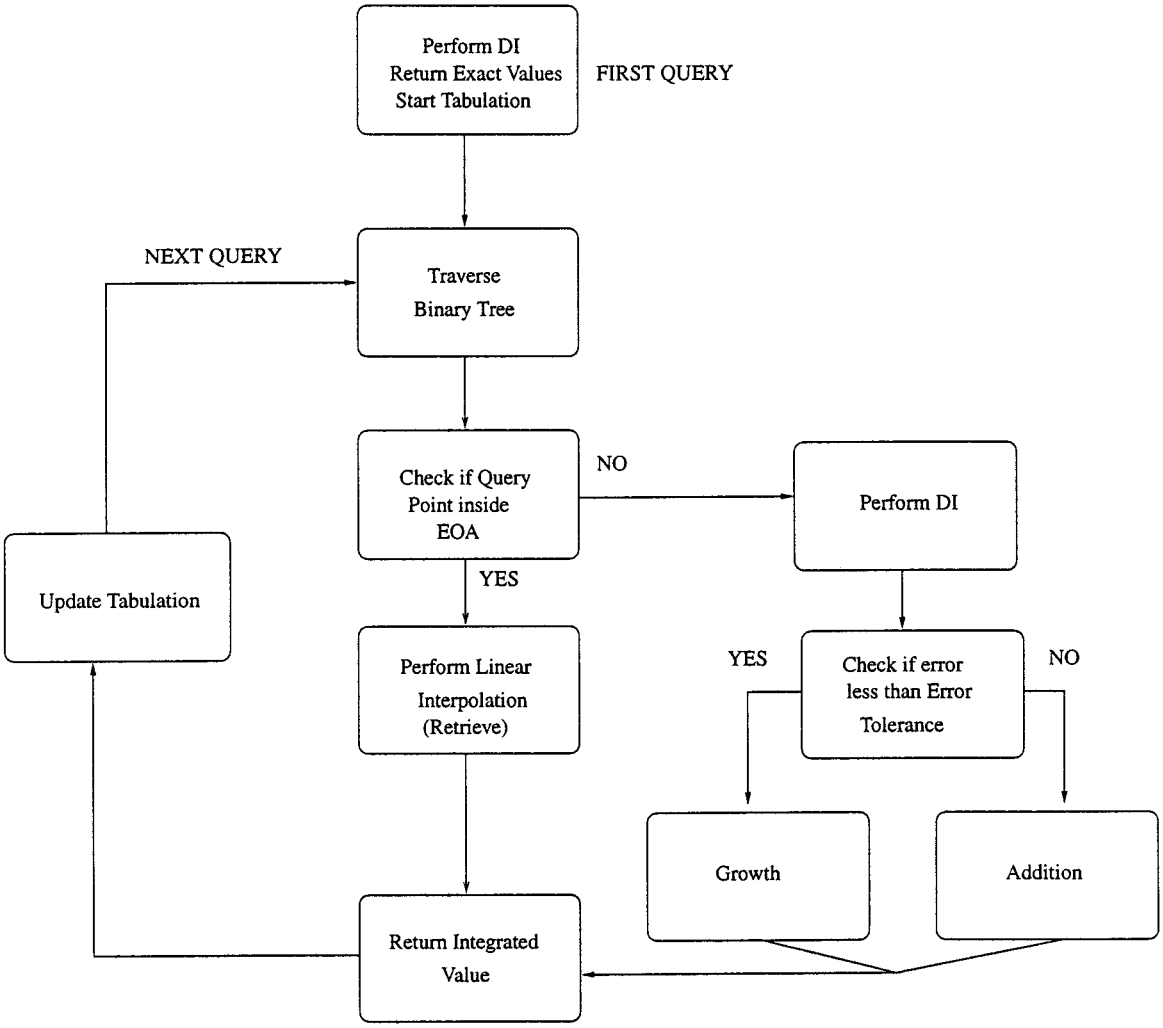

Figure 1. Flow chart representing the key steps involved in the in situ adaptive tabulation (ISAT) algorithm. At the beginning of the simulation, the binary table is empty and thus the first call begins at the point marked "FIRST QUERY". Subsequently, all calls to the algorithm begin at the point marked "NEXT QUERY". Once the binary table is mature, nearly all calls result in a "Retrieve", thereby avoiding a costly direct integration (DI) step.

ensures that the local error condition is satisfied with a minimum number of tabulated points, the growth process is a critical component of ISAT.

5. The records are stored in a binary tree which, given a query composition ϕ^q, can be traversed to obtain a table entry ϕ^0 which in some sense is close to ϕ^q. Depending on ϵ_{tol}, the new query point may or may not lie within the EOA centered at ϕ^0.

6. If the new query point is within the EOA, then eq 10 is employed to estimate the reaction mapping. This step is known as a *retrieve*.

7. If the new query point is outside the EOA, the reaction mapping is computed by DI. The mapping error ϵ is then determined and compared with the error tolerance ϵ_{tol}. If $\epsilon \leq \epsilon_{tol}$, then the EOA is expanded in a *growth* step as explained earlier. However, if $\epsilon_{tol} < \epsilon$, then the query point is tabulated as a new data point, leading to the *addition* of records in the binary table.

8. As the calculation proceeds, with increasing probability, the query composition ϕ^q lies within the EOA of a table entry ϕ^0, so that the mapping is efficiently retrieved using the linear approximation. In a typical calculation, the infancy of a newly created table is dominated by *addition*, followed by an intermediate period dominated by *growth*, until the table reaches maturity where almost every query leads to a *retrieve*. Because the retrieve step is computationally inexpensive as compared to DI, the overall computational efficiency increases dramatically once the table is mature.

5. Error Analysis

As discussed in section 4, the ISAT algorithm updates the particle composition at each time step using linear interpolation rather than direct integration (DI). This aspect of ISAT introduces estimation error in the results thus obtained. In this section, we discuss the various parameters associated with the error control and find optimum error-control parameter values for the methane thermochlorination reaction scheme.

The local error in the ISAT algorithm is defined as the difference between the reaction mapping $\mathbf{R}^{DI}(\phi)$ obtained by DI and that found using the ISAT: $\mathbf{R}^{ISAT}(\phi)$. As discussed by Pope,[15] this error is controlled satisfactorily by specifying an error tolerance ϵ_{tol}. The accuracy of the results obtained using ISAT will have a strong dependence upon ϵ_{tol}. It should also be obvious that decreasing ϵ_{tol} will increase the accuracy of the estimation, but at the cost of increased storage requirements and an increase in the overall time of the calculation. This aspect of ISAT makes the selection of an optimum ϵ_{tol} not only challenging but also interest-

Table 8. ISAT Performance for Different Values of the Error Tolerance

	ϵ_{tol}				
	1.28×10^{-2}	3.2×10^{-3}	2×10^{-4}	1.25×10^{-5}	DI[a]
total CPU time (s)	214	503	1157	4395	54543
fraction for chemistry	0.99	0.99	0.99	0.99	>0.99
average CPU time per time step	0.2	0.5	1.2	4.4	54.5
speed-up factor	254	109	48	13	
number of records	14	37	224	966	

[a] DI results are provided for comparison.

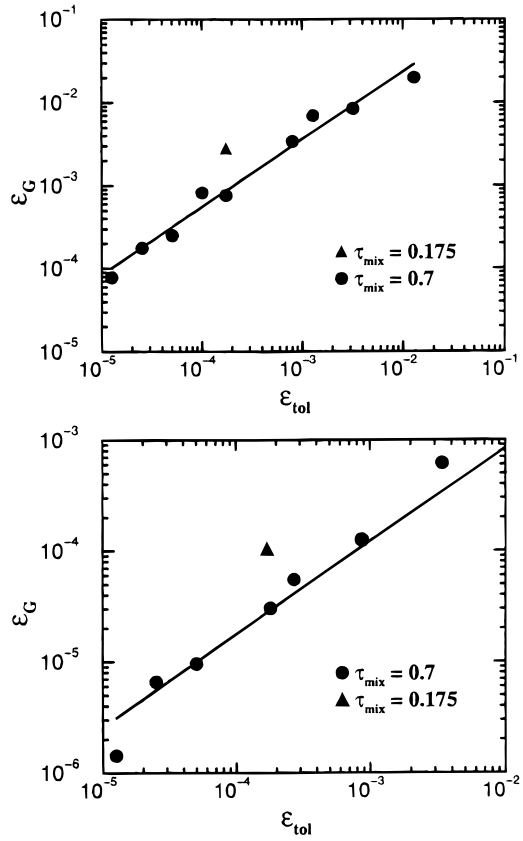

Figure 2. Effect of error tolerance on average global error based on all species (top) and average global error based only on minor species (bottom) for two different mixing times. The solid lines represent power laws fitted to the simulation data as discussed in the main text.

ing. We now discuss the detailed tests performed for eight different values of ϵ_{tol} ranging from 10^{-1} to 1.25×10^{-5}. An overview of ISAT performance is presented in Table 8, along with representative data for DI.

Error Tolerance Based on Global Error. The average global error (ϵ_G) for species combines the absolute errors incurred for major and minor species together, and is defined by

$$\epsilon_G \equiv \frac{1}{KN}\sum_{k=1}^{K}\sum_{n=1}^{N}|\phi^{(n)}(k\,\delta t) - \phi_{DI}^{(n)}(k\,\delta t)| \qquad (11)$$

where $\phi^{(n)}(k\,\delta t)$ is the composition (mole fractions) vector of the nth particle on the kth time step, and $\phi_{DI}^{(n)}(k\,\delta t)$ is the corresponding vector obtained when the entire calculation is performed using DI. Figure 2 (top) shows ϵ_G as a function of the ϵ_{tol} for the PMSR simulations. Linear interpolation from the data in the figure yields the following power-law dependency:

Table 9. Global Error Indices for the ISAT Calculations for Different Values of the Error Tolerance[a]

	ϵ_{tol}			
	1.28×10^{-2}	3.2×10^{-3}	2×10^{-4}	1.25×10^{-5}
ϵ_G	1.99×10^{-2}	8.37×10^{-3}	7.65×10^{-4}	7.86×10^{-5}
ϵ_G^{minor}	3.72×10^{-4}	6.58×10^{-4}	4.93×10^{-5}	5.96×10^{-6}
ϵ_{rel}^{major} (%)	1.45	1.01	0.59	0.045
ϵ_{rel}^{minor} (%)	274.5	52.9	16.7	15.9
ϵ_{max} (%)	2.1	1.52	0.69	0.16

[a] ϵ_G: Average global error. ϵ_G^{minor}: Average global error based on minor species. ϵ_{rel}^{major}: Average relative error in major species (%). ϵ_{rel}^{minor}: Average relative error in minor species (%). ϵ_{max}: Maximum error in any species when compared to peak value of all species (%).

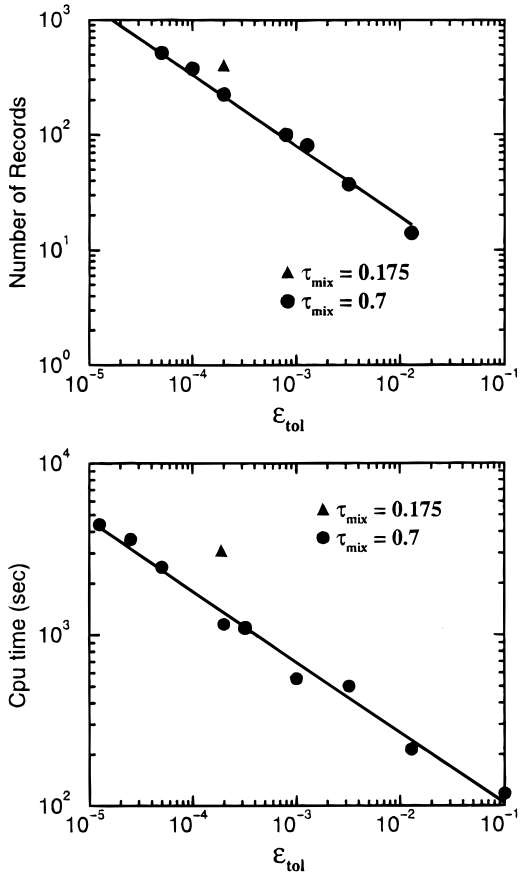

Figure 3. Effect of error tolerance on number of records stored in the binary tree (top) and total CPU time in seconds (bottom) for two different mixing times. The solid lines represent power laws fitted to the simulation data as discussed in the main text.

$$\epsilon_G = 0.99\epsilon_{tol}^{0.814} \qquad (12)$$

The average global error based only on the minor species (see Table 9) is shown in Figure 2 (bottom) and can be expressed as

$$\epsilon_G^{minor} = 0.32\epsilon_{tol}^{1.06} \qquad (13)$$

The results in Figure 2 clearly show the success of ISAT in controlling of the average global error in the PMSR simulations.

At this point it is important to point out the vast range of the compositions of the different species encountered in this test. The major species have mole fractions greater than 0.01, whereas minor species with mole fractions as low as 10^{-8} have been observed.

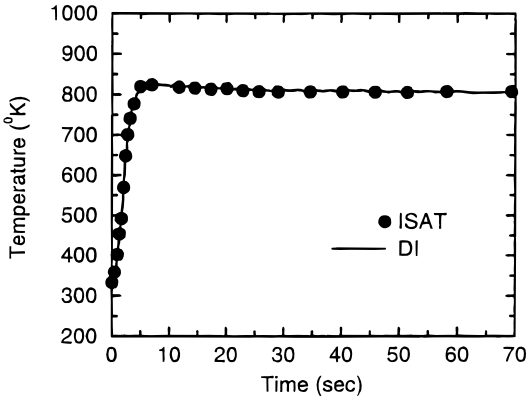

Figure 4. Time evolution of the mean temperature in the PMSR reactor found with $\epsilon_{tol} = 0.0002$ (symbols) and direct integration (solid line).

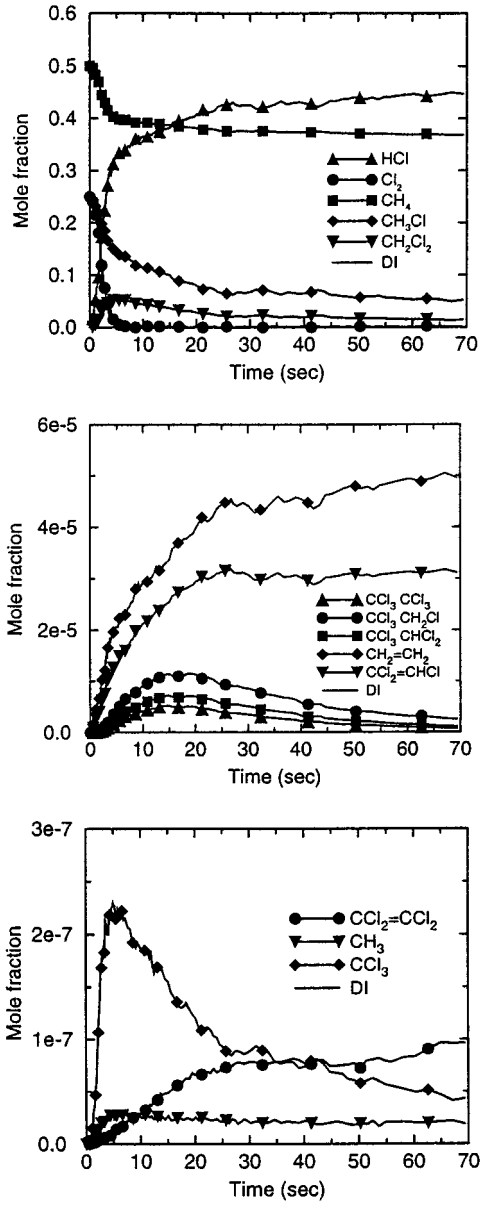

Figure 5. Time evolution of selected species mole fractions found with $\epsilon_{tol} = 0.0002$ (symbols) and direct integration (solid lines). Top: major species. Middle: minor species. Bottom: ppm species.

Taking this into consideration, one strategy to select ϵ_{tol} can be based upon the maximum average global error based on minor species only. Another strategy is to use

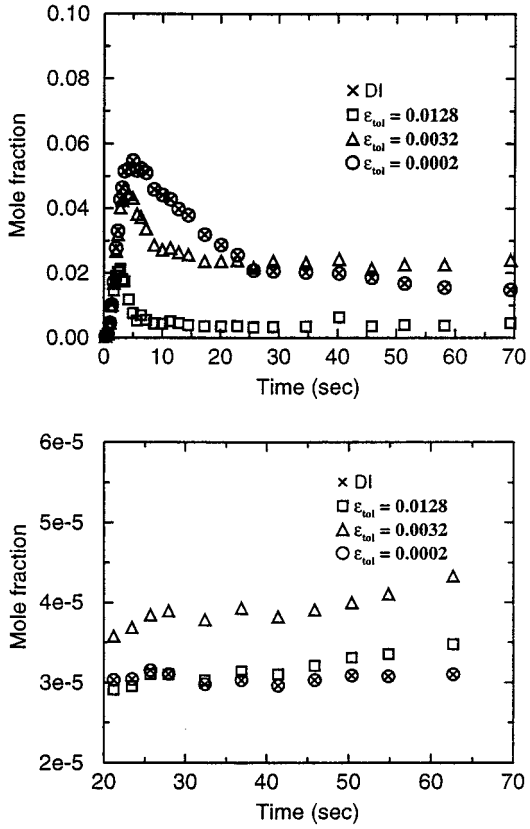

Figure 6. Effect of error tolerance on the prediction of major and minor species. Top: major species CH_2Cl_2. Bottom: minor species CCl_2=CHCl. Note that for $\epsilon_{tol} = 0.0002$ the agreement with direct integration (DI) is excellent.

the relative global error for each individual species as the criterion for optimizing ϵ_{tol}. This is particularly useful when, for example, some specific minor species are more important to the problem. We can specify the relative global error that can be tolerated for that particular species, which can then be used in eq 13 to find a good estimate of the ϵ_{tol}.

From the results obtained in these tests (see Table 9), we observe that the relative global error for the major species (i.e., with mole fractions greater than 0.01) is less than 1% when ϵ_{tol} is less than 10^{-3}. In the case of minor species, there is a much stronger dependence on ϵ_{tol}. Also, we observe that the relative global error for some particular minor species can be even more than 150%, which is justified by the fact that the absolute values of their composition are of the order of 10^{-8} or less. However, when we focus on the minor species which are at or near the ppm levels (i.e., in the range 10^{-6}–10^{-7}), we can decrease the average relative global error to as low as 16% by specifying the ϵ_{tol} to be 2×10^{-4}. For this particular ϵ_{tol}, we find that the average global error is of the order of 10^{-3}. Also, the maximum error in any species when compared to the peak value of all species is less than 0.6%.

Error Tolerance Based on Storage Requirement. The storage requirements will depend upon the number of records stored in the binary tree table. As shown in Figure 3 (top), the number of records that are stored in the table increases with the decreasing values of ϵ_{tol} according to

$$N_{table} = 1.14\epsilon_{tol}^{-0.62} \qquad (14)$$

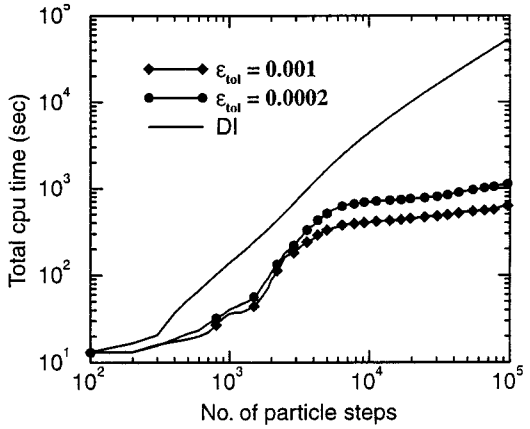

Figure 7. Total CPU time in seconds versus number of particle steps for direct integration (DI) and two different values of ϵ_{tol}.

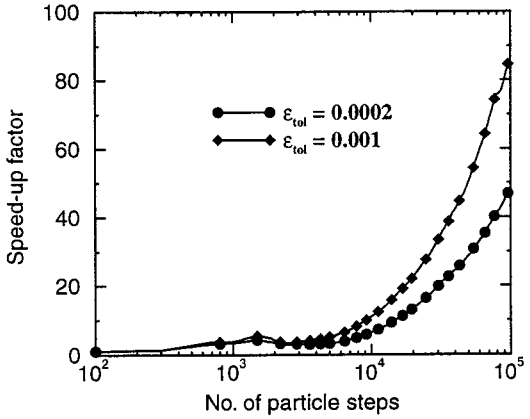

Figure 8. Speed-up factor versus number of particle steps for two different values of ϵ_{tol}.

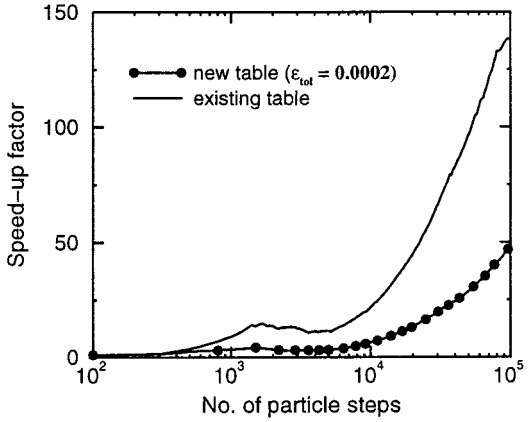

Figure 9. Comparison of speed-up factor found with an existing binary table versus a new table.

Thus, by selecting $\epsilon_{tol} = 2 \times 10^{-4}$, the number of records predicted by eq 14 is 217, which compares well with the observed value of 224. For this example, the computer memory required is only 5 MB, which essentially is due to the relative simplicity of the macroscopic flow pattern and the mixing term in the PMSR test case. However, in a preliminary full PDF simulation of a jet-stirred reactor (i.e., nearer to PFR than to CSTR behavior), the computer memory requirement was found to be of the order of 100 MB,[20] which can then be the most crucial factor for selecting the value of ϵ_{tol}. Nevertheless, in general, it is recommended that the error tolerance be set according to the chemical species, even if this means

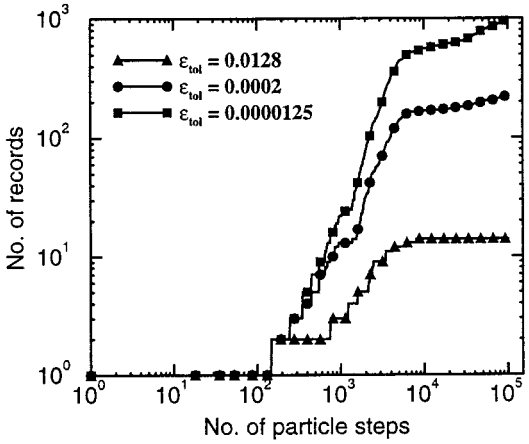

Figure 10. Number of records stored in the binary tree versus number of particle steps for three different values of ϵ_{tol}.

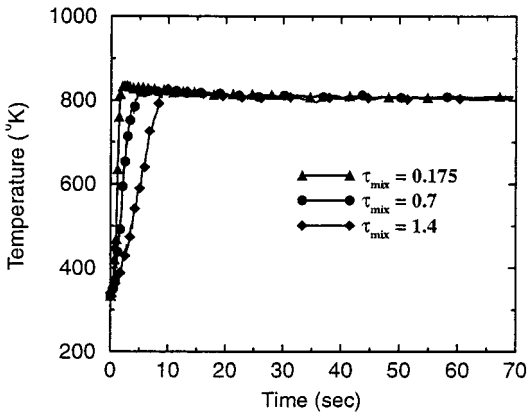

Figure 11. Time evolution of mean temperature for three different mixing times.

that the simulation must be run on a computer with larger memory.

Error Tolerance Based on Total CPU Time. As should be expected, the total CPU time also increases with decreasing ϵ_{tol} as shown in Figure 3 (bottom). The total CPU time (seconds) can be expressed as a power law by

$$T = 39.8\epsilon_{tol}^{-0.4} \tag{15}$$

Since for the PMSR model the mixing part is computationally insignificant, the chemistry part of the calculation (eq 8) accounts for more than 99% of the total CPU time. The total CPU time required for $\epsilon_{tol} = 2 \times 10^{-4}$ is about 20 min. Further discussion on the total CPU time is presented in section 6 below.

The principal conclusion, therefore, is that we can adequately control the global accuracy of the chemical species of interest by suitably choosing ϵ_{tol}. It is observed that as opposed to the major species, the minor species show a very sensitive dependence on ϵ_{tol}. Thus, we recommend that the error tolerance be selected on the basis of minor species. As will be seen in the next section, the results obtained with the PMSR model by using $\epsilon_{tol} = 2 \times 10^{-4}$ show reasonable accuracy and minimal storage requirements with a significant improvement in computational efficiency.

6. Example Results and Discussion

In this section, we present example results from the adiabatic PMSR simulations of methane thermochlori-

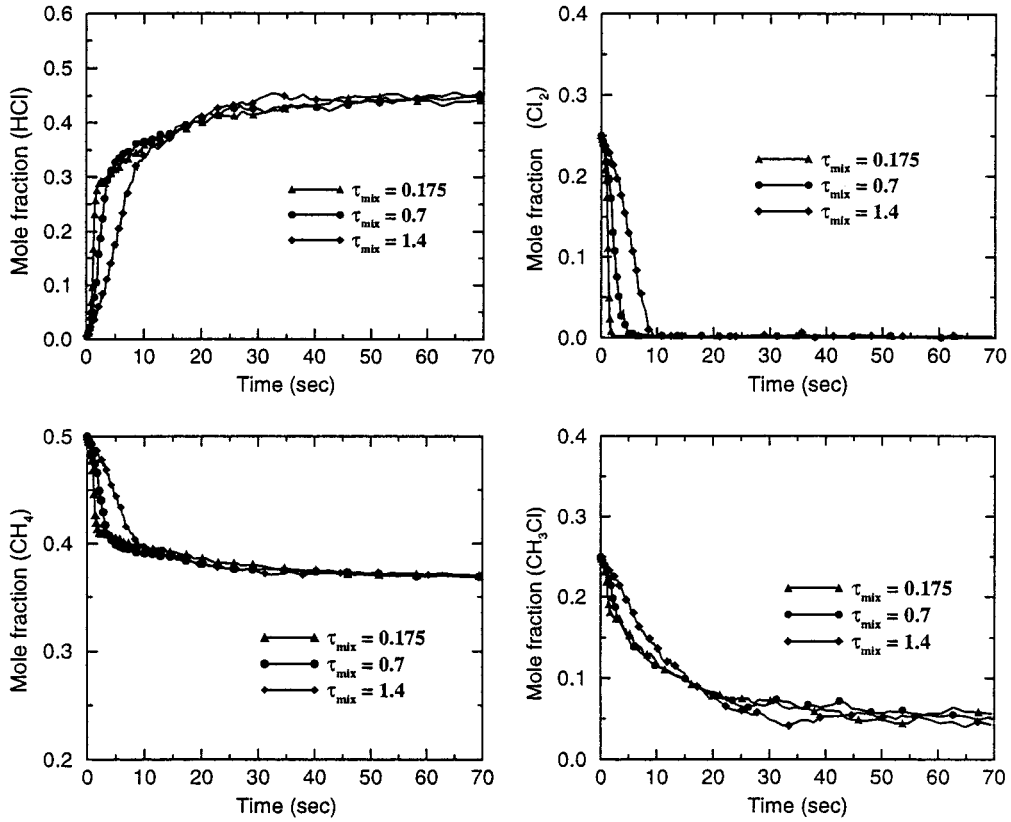

Figure 12. Time evolution of major species for three different mixing times.

nation. As noted in the Introduction, these simulations correspond to a poorly micromixed adiabatic CSTR. The inlet and initial conditions for the simulation were discussed in section 3. Unless noted otherwise, all calculations were carried out with $\epsilon_{tol} = 2 \times 10^{-4}$.

Profile of Mean Temperature. Figure 4 shows the evolution of mean temperature (i.e., arithmetic mean of the particle temperatures). The mean temperature increases from the initial temperature of 333 K and reaches a steady-state value of 807 K within the first 5 s. The small fluctuations that can be observed in the curve are entirely due to the stochastic nature of the PMSR test case and in no way reflect an error of any kind.

Profile of Major and Minor Species. Figure 5 shows the comparison between predictions by ISAT and DI for the profile of mean mole fractions of the major (top) and minor species. Figure 5 (middle) shows the profile of selected minor species with mole fractions of the order of 10^{-5}, and Figure 5 (bottom) is for the minor species at ppm level. The results show a very good match with the DI results for the major species and minor species, even at ppm levels or smaller. The observed fluctuations in the curves are again due to the random nature of the mixing terms in the PMSR model.

Effect of Error Tolerance on the Profile of Major and Minor Species. Figure 6 shows the predictions of a major species CH_2Cl_2 (top) and a minor species CCl_2=CHCl (bottom) for the following values of ϵ_{tol}: 1.28×10^{-2}, 3.2×10^{-3}, and 2×10^{-4}. The corresponding values found using DI are included for comparison. As expected, the level of accuracy for the ISAT predictions increases with decreasing ϵ_{tol}. We see that satisfactory levels of accuracy are achieved with $\epsilon_{tol} = 2 \times 10^{-4}$ and the results nearly coincide with the DI values. Similar agreement is observed for all other species with $\epsilon_{tol} = 2 \times 10^{-4}$.

Performance of ISAT. From Figure 7, we see that the total CPU time for the entire calculation (1000 time steps) is about 20 min when $\epsilon_{tol} = 2 \times 10^{-4}$ is used to the control of error. For similar operating conditions, the same calculation takes about 17 h when DI is used. This more than adequately demonstrates the significant gains in computational efficiency achieved by implementation of ISAT. When ϵ_{tol} is increased to 10^{-3}, the total CPU time for ISAT decreases to about 10 min. A parameter that has been used[15,19] to evaluate the performance of ISAT is the speed-up factor defined by

$$\text{speed-up factor} = \frac{\text{CPU time for } Q \text{ queries using DI}}{\text{CPU time for } Q \text{ queries using ISAT}} \quad (16)$$

Figure 8 shows the speed-up factor for the two different values of ϵ_{tol}. We observe that during the initial stages of the calculation, the speed-up factor increases rather gradually, but after 10^4 particle steps, there is a significant rise in the speed-up factor. In terms of the storage, this result implies that after about 10^4 particle steps the binary tree is mature and no new records have to be added, with subsequent calculations being performed only by multilinear interpolation (i.e., a retrieve step). Due to this, the speed-up factor rises steadily and a speed-up of 84 is achieved at the end of 1000 time steps when $\epsilon_{tol} = 10^{-3}$ is specified. The ISAT technique also allows the use of an existing binary tree table to perform the new calculations. This is advantageous in cases where the initial conditions do not vary appreciably. As shown in Figure 9, we can boost the speed-

up factor for $\epsilon_{tol} = 2 \times 10^{-4}$ from 48 to about 140 by using this method.

Storage Requirements. As shown in Figure 10, because all particles have the same initial conditions, the number of records remains unity up to 100 particle steps. We then observe a rapid buildup of the binary table until about 10^4 particle steps (i.e., about 7 s), after which the table size remains almost constant. As discussed earlier, the speed-up curves clearly reflect these features whence rapid table buildup is accompanied by a slowing of the calculations and an asymptotic increase of speed-up when the table buildup curve flattens. Note that the buildup period roughly corresponds to the rapid initial transient in the mean temperature (Figure 4). Thus, the major part of the calculation is carried out in the regime where the binary table is mature.

Effect of Mixing Time. From results obtained by varying the mixing time at a constant residence time, we have found that the mixing time has a significant effect only in the initial stages of the simulation. As seen in Figure 11, the increase in temperature is more gradual when the mixing time is longer (i.e., 1.4 s) than when the mixing time is shorter (i.e., 0.175 s). However, the final steady-state temperature value (807 K) is independent of the mixing time. We observe similar behavior in the prediction of major species (see Figure 12) where the effect of mixing time is visible only in the initial stages of the simulation. However, we observe a violation of this pattern in the prediction of minor species CCl_3-CCl_3 and $CH_3^{\bullet}$ (see Figure 13). Indeed, it would appear that faster molecular scale mixing (i.e., smaller τ_{mix}) favors the production of CCl_3-CCl_3 in a perfectly macromixed adiabatic CSTR. We plan to explore this finding in greater detail using full PDF simulations of a jet-stirred reactor. For this reactor, both large-scale inhomogeneities and micromixing will have a significant effect on the product distribution. As noted earlier, our preliminary results for the jet-stirred reactor indicate that product distribution depends not only on the flow field but also on how the reaction mixture is cooled due to external heat transfer.

As can be seen in Figure 2, the global error increases for the case with the smaller mixing time because of the increase in the number of iterations that have to be performed to attain the same simulation time (i.e., K is eq 11). As shown in Figure 14, the number of records that are added to the binary table generally increases with a decrease in mixing time. The increase in number of additions explains the increase in the CPU time when the mixing time is decreased as seen in Figure 3. On account of this, the speed-up factor increases from 48 to 89 when the mixing time decreases from 0.7 to 0.175 s (Figure 15). In general, the effect of mixing time is difficult to predict a priori since it will depend on its value relative to the chemical time scales present in the chemical kinetic scheme. This effect is evident in Figure 14, where the number of records jumps from just over 200 when $\tau_{mix} = 0.7$ to over 300 when $\tau_{mix} = 0.5$. Notice also from Figure 14 that the change in the number of records is not monotone with respect to τ_{mix}.

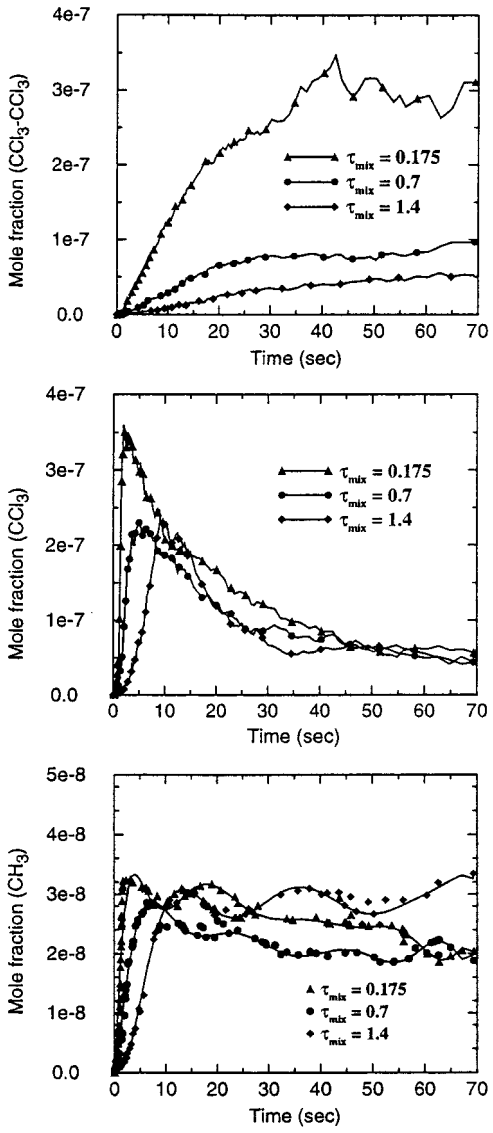

Figure 13. Time evolution of minor species for three different mixing times.

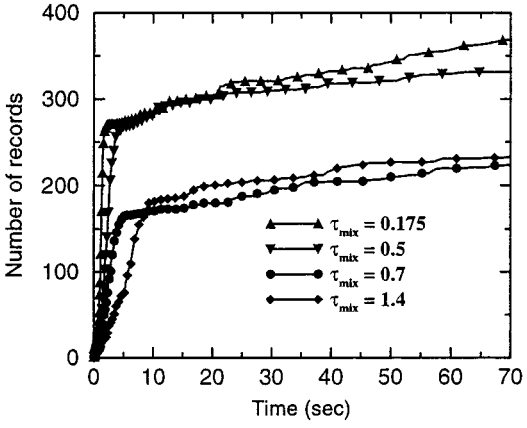

Figure 14. Time evolution of number of records stored in the binary tree for four different mixing times.

7. Conclusions

The results presented here demonstrate that the implementation of ISAT makes possible the hitherto formidable task of implementing detailed chemistry in CFD simulations of methane thermochlorination reactors. Indeed, using a detailed chemical kinetic scheme and a detailed flow model based on CFD, it is now possible to predict the minor species occurring at any location within the reactor even at ppm levels with reasonable computational cost. Using an error tolerance

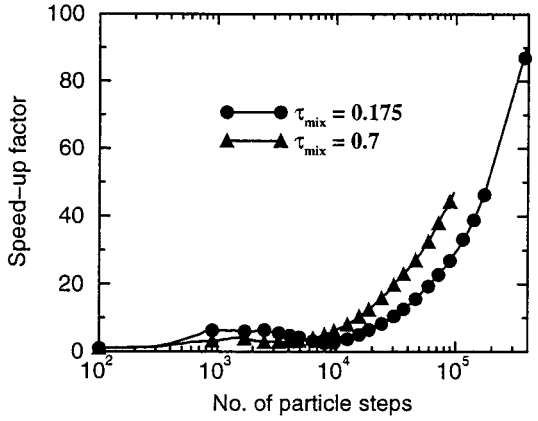

Figure 15. Speed-up factor versus number of particle steps for two different mixing times.

of $\epsilon_{tol} = 2 \times 10^{-4}$, we have obtained sufficiently accurate results with minimal storage requirements and significantly less computational time than would be required with direct integration. On the basis of numerous test simulations, we conclude that an error tolerance in the range of 10^{-3}–10^{-4} is satisfactory for carrying out full PDF simulations of methane thermochlorination reactors. In the PMSR, a speed-up of up to 138 over direct integration can be achieved by specifying the same error tolerance, and similar speed-up is expected in full PDF simulations. In a future communication, full PDF simulation results for methane thermochlorination in a jet-stirred reactor will be reported. Initial results[20] suggest that the speed-up observed in full PDF simulations is very similar to that observed here for the PMSR model. Finally, the implementation of ISAT reported in this work is in no way limited to methane thermochlorination kinetics. Indeed, in our research group it has also been successfully employed for full PDF simulations of free-radical polymerization of ethylene using a detailed kinetic scheme including ethylene decomposition,[7] and can be easily implemented for other kinetic schemes such as the 116 species/447 reaction Exxon model.[21]

Acknowledgment

The authors thank Prof. S. B. Pope and Dr. K. Tsai for many useful comments concerning the implementation of ISAT. They are also indebted to Drs. S. Sen, M. Tirtowidjo, and D. H. West at The Dow Chemical Company for suggesting the methane thermochlorination reactor as an industrially relevant test case. This work was supported by the National Science Foundation under Grant CTS-9720205 (CTS-9996242) and the Kansas Program for Complex Fluid Flows.

Literature Cited

(1) Wiseman, P. *An Introduction to Industrial Organic Chemistry*, 1st ed.; Wiley: New York, 1972.

(2) Reed, D. J. *Encyclopedia of Chemical Technology*, 4th ed.; Kroschwitz, J. I., executive Ed., Howe-Grant, Mary, Ed.; Wiley: New York, 1991.

(3) Facts and Figures for the Chemical Industry. *Chem. Eng. News* **1996**, *76* (24), 38.

(4) Tirtowidjo, M. Fundamental Kinetic Modeling of Industrial Reactors. AIChE Annual Meeting, Los Angeles, November 1997; paper 78b.

(5) Fox, R. O. Computational Methods for Turbulent Reacting Flows in the Chemical Process Industry. *Rev. Inst. Fr. Pét.* **1996**, *51*, 215.

(6) Deutschmann O.; Schmidt, L. D. Modeling the Partial Oxidation of Methane in a Short-Contact-Time Reactor. *AIChE J.* **1998**, *44*, 2465.

(7) Kolhapure, N.; Fox, R. O. CFD Analysis of Micromixing Effects on Polymerization in Tubular Low-Density Polyethylene Reactors. *Chem. Eng. Sci.* **1999**, *54*, 3233.

(8) Tsai, K.; Fox, R. O. PDF Modeling of Turbulent-Mixing Effects on Initiator Efficiency in a Tubular LDPE Reactor. *AIChE J.* **1996**, *42*, 2926.

(9) Petzold, L.; Zhu, W. Model Reduction for Chemical Kinetics: An Optimization Approach. *AIChE J.* **1999**, *45*, 869.

(10) Liu, C. H.; Barkelew, C. H. Numerical Analysis of Jet-Stirred Reactors with Turbulent Flows and Homogenous Reactions. *AIChE J.* **1985**, *32*, 1813.

(11) Roekaerts, D. Use of a Monte Carlo PDF Method in a Study of the Influence of Turbulent Fluctuations on Selectivity in a Jet-Stirred Reactor. *Appl. Sci. Res.* **1991**, *48*, 271.

(12) Acharya, S.; Jang, D. S.; West, D. H.; Hebert, L. A. A Moment Closure Method for Modeling a Multistep Chlorination Reaction. AIChE Spring National Meeting, March 1991; paper 33a.

(13) Sen, S. Private communication.

(14) Pope, S. B. PDF Methods for Turbulent Reactive Flows. *Prog. Energy Combust. Sci.* **1985**, *11*, 119.

(15) Pope, S. B. Computationally Efficient Implementation of Combustion Chemistry Using *In Situ* Adaptive Tabulation. *Combust. Theory Modell.* **1997**, *1*, 41.

(16) Beam Technologies Inc. *ISAT-CK User's Guide (Release 1.0)*; Beam Technologies Inc.: Ithaca, NY, 1998.

(17) Yang, B.; Pope, S. B. An Investigation of the Accuracy of Manifold Methods and Splitting Schemes in the Computational Implementation of Combustion Chemistry. *Combust. Flame* **1998**, *112*, 16.

(18) Kee, R. J.; Rupley, F. M.; Miller, J. A. Chemkin-II: A Fortran Chemical Kinetics Package for the Analysis of Gas phase Chemical Kinetics. *Sandia Rep.* **1989**, *SAND89-8009B*.

(19) Saxena, V.; Pope, S. B. PDF Simulations of Turbulent Combustion Incorporating Detailed Chemistry. *Combust. Flame* **1998**, *117*, 340.

(20) Shah, J. J.; Fox, R. O. An Efficient Algorithm for Full PDF Simulation of Methane Thermochlorination Reactions. AIChE Annual Meeting, Miami, November 1998; paper 318p.

(21) Mims, C. A.; Mauti, A. M.; Dean, A. M.; Rose, K. D. Radical Chemistry in Methane Oxidative Coupling: Tracing Ethylene Secondary Reactions with Computer Models and Isotopes. *J. Phys. Chem.* **1994**, *98*, 13357.

Received for review February 22, 1999
Revised manuscript received August 16, 1999
Accepted August 18, 1999

IE990125G